

This is a pre print version of the following article:

Modelling local climate change using site-based data / Morlini, Isabella; Franco-Villoria, Maria; Orlandini, Stefano. - In: ENVIRONMENTAL AND ECOLOGICAL STATISTICS. - ISSN 1352-8505. - 30:2(2023), pp. 205-232. [10.1007/s10651-023-00560-z]

Terms of use:

The terms and conditions for the reuse of this version of the manuscript are specified in the publishing policy. For all terms of use and more information see the publisher's website.

18/12/2025 17:59

Modelling local climate change using site-based data

Isabella Morlini^{1†}, Maria Franco-Villoria^{1†} and Stefano
Orlandini^{2†}

^{1*}Department of Economics Marco Biagi, University of Modena
and Reggio Emilia, Italy.

^{2*}Department of Engineering Enzo Ferrari, University of Modena
and Reggio Emilia, Italy.

*Corresponding author(s). E-mail(s): isabella.morlini@unimore.it;

Contributing authors: maria.francovilloria@unimore.it;

stefano.orlandini@unimore.it;

[†]These authors contributed equally to this work.

Abstract

In the context of the ongoing United Nations Framework Convention on Climate Change (UNFCCC) process, it seems important to focus attention not only on global mean surface air temperature (GSMT) but also on climate of specific regions, in order to gain insights into the dynamics of the changes, the timescales of the periodic components, the local trends and the relationships between climatic variables in the region of interest. This is important for scientists as well as for policy makers. This paper provides an analysis of the changes in local air temperature and precipitation depth in exceptionally long observational records and examines the relationships between these two variables. The focus is on monthly values. Temperature maximum, minimum and range and cumulative precipitation depth are considered. The wavelet analysis shows that the scale of variation is different for temperature and precipitation and that the behaviour of the temperature range values diverges from the behaviour of the minimum and maximum values. The timescale of important changes in the long-term trend is, however, similar. Results also suggest that the main mode of variability is persistent through time in the series of temperature maximum, minimum and range but not in precipitation depth. This is a clear evidence of climate change. All series

show variances that change over time and are, as expected, nonstationary. The analysis of the wavelet coherence shows that the relationship between precipitation and temperature evolves through time, and its intensity varies considering different time scales. The association between these climatic variables is particularly strong in the last decade. Noteworthy, the analysis of the coherence suggests that is temperature leading rain and not the other way around. This highlights the impact of global warming on hydrologic cycle and on related human activities.

Keywords: Air temperature, Climate interactions, Precipitation depth, Wavelet analysis

1 Introduction

The subject of climate change usually focuses attention on global mean surface air temperature both for analysing temperature change [1–4] and for estimating relationships between temperature and climate forcing mechanisms like carbon dioxide and solar irradiance [5, 6]. However, it is the change on regional and local scales that affect people directly and the knowledge of this change is essential for the development of adaptation strategies and policy makers intervention [7]. Geophysical local time series are often generated by complex systems of which we know little about and predictable behavior in such systems like trends and periodicities are therefore of great interest (see, among others, [8]). In this paper we examine historical variations in local surface air temperature and precipitation depth using data from the Geophysical Observatory of the University of Modena and Reggio Emilia (Italy). These data can provide uncommon evidence of the long-term trend and of the relationships between temperature and precipitation which are hard to find in any global investigation due to the scarcity of long observed (and not simulated) time series. Discrete and continuous wavelets are used to characterize the time series and to study the association between temperature and precipitation, to compare the features of these climatic variables and to detect the abrupt shifts in both cyclic and trend dynamics. The tools of the discrete and continuous wavelet transforms [9, 10], the wavelet spectra, coherence, and phase offer a comprehensive assessment of the characteristic modes of variability of climate system forcing and of the scale-based relationships between natural climate variables. In addition, short-term variations in local surface temperature and rain can be associated with internally generated natural climate variability and external climate forcing, while long-term variations are strongly related to human-induced changes only [11]. In particular, the research questions, addressed in this work, are:

1. Which frequencies contribute the most to the variability of the series? Do the periodicities remain constant or evolve in time? Are these periodicities the same in temperature and precipitation?

2. How does the long-term trend evolve in time? Is there a point of an important discontinuity?
3. At which timescales, if any, temperature and precipitation have a common behaviour? Has the association between these two variables changed in the last decade? Which variable influences the other one?

Giving an answer to these questions means exploring systematically weather changes and the relationships between variations in temperature and precipitation. Even though the annual cumulative precipitation depth and the annual maximum and minimum temperature do not show evident dynamics in time, the study of climate change requires consideration and comparison of both the internal variability in the local system and the behaviour due to a global development. Wavelet analysis is used here to separate the contribution of these two factors by reconstructing the original time series as a sum of detailed components, each of which corresponds to an oscillating component with a different period that can be associated to local variations, and a smooth component showing the long-term trend, that can be associated to a global dynamic.

The rest of the paper is organized as follows. Section 2 illustrates the data and methods. Section 3 reports and discusses results of the statistical analyses. Conclusions and directions for future research are reported in Section 4.

2 Data and methods

2.1 Data

The monthly time series of maximum and minimum air temperature T_{max} and T_{min} and temperature range $Trange$ (°C) and cumulative precipitation depth PMM (mm) are obtained from uninterrupted daily observations collected from 1-01-1861 to 31-12-2020 at the Geophysical Observatory of the University of Modena and Reggio Emilia (latitude 44.6474N, longitude 10.9293E, elevation 76.50 m asl), Modena, Italy. These long term in situ observations (160 years, 1920 monthly observations per series) are not affected by in-homogenities caused by changes in instrumentations, station moves, different observing practices (for example, different formulas for calculating the minimum and the maximum) or different observations time. Therefore, observed variability is due to changes in the local and global environment and can be related to global CO₂ as well as to variations in the local development. T_{max} and T_{min} are defined as the maximum and minimum daily value in the month, respectively, while $Trange$ is the monthly average of the daily temperature range values. While changes in the maximum and minimum temperatures are strongly associated with changes in the average temperature, temperature range provides additional information for observing climate variability and change [12, 13]. For this reason, in this study we also consider the monthly average of the difference between daily maximum temperature and minimum temperature, as it has been shown to be an important meteorological indicator associated with global climate change. PMM is defined as the cumulative precipitation depth

in the month. There are 9 missing values in precipitation in 1943 that are imputed using cubic spline interpolation.

2.2 Methods

To extract information and to identify scales of variation in the series we use the wavelet analysis. In order to uncover the different characteristics of the series we apply both discrete and continuous wavelets. We use a modified version of the classic Daubechies wavelet for the discrete analysis [14–17] called “least asymmetric” (LA), and the Morlet wavelet for the continuous analysis. The LA filter is a common choice in practical applications (see, for example [18]). For a comparison of different continuous wavelets in an ecological contest we refer to [19]. All the analysis are carried out with R [20], using the R packages `wavelets` [21], `biwavelet` [22] and an advanced version of the latter [23], available at the website of the author.

We first use the discrete wavelet transform (DWT) to perform a spectral analysis assuming stationarity, in order to partition the variance of the series into its different oscillating components with different frequencies (periods) and to detect which frequencies contribute the most to the variance of the series. We then use the discrete wavelet for a non-stationary analysis by performing a local time-scale decomposition of the series and estimating the spectral characteristics as a function of time [9, 24]. Further, we use the continuous wavelet transform (CWT) approach that is more suited for the extraction of local time-scale or time-frequency information and it is characterized by a well-defined relationship between frequency and scale [25]. As shown in [26], while discrete wavelets are more indicated for the representation of the process on appropriate bases and the relationship between scale and frequency in this approach has less meaning, the main feature of continuous wavelets is the time-frequency decomposition with the optimal trade-off between time and frequency resolution, which permits investigation of the temporal evolution of aperiodic and transient processes. Last, we use the continuous wavelet coherence for a bi-variate analysis of the time series, in order to detect and quantify the non stationary association between precipitation and temperature.

2.2.1 Wavelet transform

The wavelet transform decomposes a signal over dilated and translated functions of the so called “mother wavelet” $\phi(t)$ [10] that can be expressed as a function of two parameters, one for the time position, τ , and one for the scale of the wavelet, a . More formally, wavelets are defined as $\phi_{a,\tau}(t) = a^{-1/2}\phi\left(\frac{t-\tau}{a}\right)$. The wavelet transform of a time series $x(t)$ of length T ($t = 1, \dots, T$), with respect to a chosen mother wavelet is performed as follows:

$$W_x(a, \tau) = \frac{1}{\sqrt{a}} \int_{-\infty}^{\infty} x(t) \phi^* \left(\frac{t - \tau}{a} \right) dt = \int_{-\infty}^{\infty} x(t) \phi_{a,\tau}^*(t) dt \quad (1)$$

where $*$ denotes the complex conjugate form. The wavelet coefficients $W_x(a, \tau)$ represent the contribution of the scales (the a values) to the signal at different time positions τ . The wavelet transform can be thought of as a cross-correlation of a signal $x(t)$ with a set of wavelets of various widths or scales a at different time positions τ . The wavelet function is not arbitrary. It is rather normalized to have unitary variance so that $\int |\phi(t)|^2 dt = 1$ and it verifies $\int \phi(t) dt = 0$. The wavelet decomposition is therefore a linear representation of the series where the variance is preserved. The original series can be recovered by using the following inverse transform:

$$x(t) = \int_{-\infty}^{\infty} \int_0^{\infty} \frac{1}{a^2} W_x(a, \tau) \phi_{a,\tau}(t) dt da \Big/ \int_0^{\infty} \|\Phi(f)\|^2 / f df \quad (2)$$

where $\Phi(f)$ denotes the Fourier transform of $\phi(t)$. Therefore, the wavelet transform is just a linear filter whose response function is given by the wavelet function. By means of (2), the original series can be reconstructed by integrating over all scales and locations. However, the integration can be limited over a chosen range of scales $a_1 - a_2$, to perform a band-pass filtering of the original time series in this chosen range. This analysis is called multiresolution analysis (MRA). In the discrete domain, the scale and shift parameters are discretized as $a = a_0^m$ and $\tau = n\tau_0$, with $a_0 > 1$ and $\tau_0 \neq 0$ to restrict the values of the parameters to a discrete sublattice (see [14]). The wavelets are also discretized, as follows:

$$\phi_{m,n}(t) = a_0^{-m/2} \phi\left(\frac{t - n\tau_0}{a_0^m}\right) \quad (3)$$

where n and m are integer values. The discrete wavelet transform and its inverse transform are defined as follows:

$$W_{m,n} = \int_{-\infty}^{\infty} \phi_{m,n}^*(t) x(t) dt, \quad (4)$$

$$x(t) = k_\phi \sum_m \sum_n W_{m,n} \phi_{m,n}(t) \quad (5)$$

where k_ϕ is a constant value for normalization. The function $\phi_{m,n}(t)$ provides sampling points on the scale-time plane that are linear sampling in the time direction but logarithmic in the scale (a -axis) direction. The scales are on a dyadic base since a_0 is chosen as $a_0 = 2^j$ where j is an integer value. This is analogous to the use of a set of narrowband filters in conventional Fourier analysis.

2.2.2 Mother wavelet

In our application, for the discrete analysis we use a modified version of the Daubechies wavelet, called least asymmetric (LA). This wavelet is the orthogonal wavelet with a phase response that most closely resembles a linear phase

6 *Modelling local climate change using site-based data*

filter; this allows to align the filtered series in time with the original series. The wavelets in the least asymmetric family have compact support and are indexed by a parameter N proportional to the regularity since, as N increases, the wavelet become smoother. In our application, $N = 8$. The wavelet is defined as follows:

$$\phi(t) = \sum_{k=-\infty}^{\infty} \beta_k \sqrt{2} \psi(2t - k) \quad (6)$$

where $\psi(t)$ is a compactly supported scaling function, $\psi(t) = \sum_{k=-\infty}^{\infty} \alpha_k \sqrt{2} \psi(2t - k)$ for the progression $\{\alpha_k\}$, k real integer, satisfying the following conditions for all integers $N \geq 2$:

$$\alpha_k = 0 \text{ if } k < 0 \text{ or } k > 2N \quad (7)$$

$$\sum_{k=-\infty}^{\infty} \alpha_k \alpha_{k+2m} = \delta_{0m}, \text{ for all integers } m \quad (8)$$

where δ_{0m} is the Kronecker delta,

$$\sum_{k=-\infty}^{\infty} \alpha_k = \sqrt{2} \quad (9)$$

$$\sum_{k=-\infty}^{\infty} \beta_k k^m = 0, 0 \leq m \leq N - 1 \quad (10)$$

where $\beta_k = (-1)^k \alpha_{-k+1}$. The function (6) satisfies the N vanishing moments condition $\int \phi(t) t^m dt = 0$, for all integers $0 \leq m \leq N - 1$. This last property has important implications for applications since it ensures that fine-scale wavelet coefficients will only be large where a function or its derivatives have singularities [25]. Another important feature is that the wavelet compact bases are capable of representing various classes of functions more efficiently than Fourier bases [27]. If we consider, as an example, a piecewise continuous function, many Fourier basis functions are needed to represent the discontinuities accurately and the effects of these basis functions will be global. On the other hand, wavelets will be able to represent the discontinuities more efficiently and at the same time they will be local and will not affect the global representation. The DWT has some limitations in terms of sample size (it has to be a power of two), and the starting point and filter choice can have an impact on the wavelet transform of the series. Instead, we use the maximum overlap DWT (MODWT); this is no longer an orthogonal transformation which means a higher computational cost, but without the issues that the DWT has [10]. In either case, for a given level of decomposition J , the original series can be re-expressed as the sum of a number of wavelet details components \mathbf{D}_j , $j = 1, \dots, J$ and a smooth component \mathbf{S}_J . The wavelet detail \mathbf{D}_j can be seen as a time series related to variations in the original time series at a scale of 2^{j-1} months, $j = 1, \dots, J$, while the smooth component \mathbf{S}_J can be interpreted

as a time series related to variations in X at scale of 2^J and higher, so one could think about \mathbf{S}_J as the long-term trend.

For the continuous analysis we utilize the mostly used Morlet mother function, defined as follows:

$$\phi(t) = \pi^{-1/4} e^{i\omega_0 t} e^{-t^2/2} \quad (11)$$

where ω_0 is the non dimensional frequency taken to be 6 to satisfy the admissibility conditions. For $\omega_0 = 6$, the second term in the Fourier transform of (11):

$$\Phi(\omega) = e^{(-\omega - \omega_0)^2/2} - e^{-\omega^2/2} e^{-\omega_0^2/2} \quad (12)$$

is so small that it can be neglected in practice and the Morlet wavelet can be consequently considered as a modulated Gaussian waveform. Another characteristic of the Morlet wavelet is that the relation between the frequency f and the scale parameter a can be derived analytically and $\frac{1}{f} = \frac{4\pi a}{\omega_0 + \sqrt{2 + \omega_0^2}}$ with ω_0 the central angular frequency of the wavelet ($\omega_0 = 2\pi f_0$). With ω_0 around 2π the scale a is inversely proportional to the frequency f . This greatly simplifies the interpretation of the wavelet analysis and one can replace, in all results, the scale a by the frequency f or the period $1/f$. With $\omega_0 = 6$ the Fourier period p_F is almost equal to the scale, since $p_F = 1.03a$ ([9]).

2.2.3 Wavelet power spectra and cone of influence

Following the previous paragraph, the scale a is replaced by the frequency f in the notation that follows. Considering the wavelet transform of a time series $x(t)$ defined in (1), we can obtain the local wavelet power spectrum, which gives the indication of how volatile a time series is across different time scales, as follows:

$$S_x(f, \tau) = \|W_x(f, \tau)\|^2 \quad (13)$$

Since we are dealing with finite-length time series, errors will occur at the beginning and end of the wavelet power spectrum as the transform assumes the data is cyclic. As the wavelet gets closer to the edge of the time series, parts of it exceed the edge and thus the values of the wavelet transform are affected creating boundary effects. The affected region increases in extent as the scale a (or the frequency f) increases. This zone where edge effects are present is called “cone of influence” and the spectral information in the cone lacks in accuracy and should be interpreted with caution. The Fourier spectrum of a series, assuming stationarity, can be related to the global wavelet power spectrum which is defined as the averaged variance contained in all wavelet coefficients of the same frequency f or scale a :

$$\bar{S}_x(f) = \frac{\sigma_x^2}{T} \int_0^T \|W_x(f, \tau)\|^2 dt \quad (14)$$

8 *Modelling local climate change using site-based data*

with σ_x^2 the variance of the time series $x(t)$ and T the length of the series. Another interesting computation is the mean variance at each time location, obtained by averaging the frequency components:

$$\bar{s}_x(\tau) = \frac{\sigma_x^2 \pi^{1/4} T^{1/2}}{\int_0^\infty \|\Phi(f)\|^2 / f df} \int_0^\infty \left(\frac{1}{f}\right)^{1/2} \|W_x(f, \tau)\|^2 df \quad (15)$$

where $\Phi(f)$ is the Fourier transform of $\phi(t)$. This quantity can also be filtered in a chosen frequency band (or range of scales) to perform a multiresolution analysis.

2.2.4 Wavelet coherence and phase difference

For the bi-variate analysis, we use the wavelet coherence. In Fourier analysis, the coherence is used to determine the association between two time series. The coherence function is a direct measure of the correlation between the spectra of two time series. To quantify the relationship between two non stationary series, one can compute the wavelet coherence. Following [28], we define the wavelet coherence between two time series $x(t)$ and $y(t)$ as the cross spectrum $W_{x,y}(f, \tau) = W_x(f, \tau)W_y^*(f, \tau)$ with $*$ denoting the complex conjugate, normalized by the spectrum of each series:

$$R_{x,y}(f, \tau) = \frac{\|\langle W_{x,y}(f, \tau) \rangle\|}{\|\langle W_{x,x}(f, \tau) \rangle\|^{1/2} \|\langle W_{y,y}(f, \tau) \rangle\|^{1/2}} \quad (16)$$

where the symbol $\langle \rangle$ denotes a smoothing operator in both time and scale. $R_{x,y}(f, \tau)$ is bounded in $[0, 1]$. The smoothing is performed by a convolution with a constant length window function both in the time and frequency direction [29]. For the Morlet wavelet, the most suited smoothing operator having

similar footprint as the wavelet, is given in [28]. It is $\left(W_{x,y}(f, \tau) * c_1^{-\frac{t^2}{2f^2}} \right) \Big|_f$

for the frequency and $(W_{x,y}(f, \tau) * c_2 \Pi(0.6a))|_\tau$ for time, where c_1 and c_2 are normalization constants and Π is the rectangle function. The factor 0.6 is an empirically determined scale decorrelation length. In practice both convolutions are done directly and the normalization coefficients are determined numerically. The advantage of these quantities based on wavelets is that they vary in time and can also detect transient correlations between two series. The wavelet coherence provides information about at which temporal location and frequency two non stationary time series are linearly correlated. The quantity $R_{x,y}(f, \tau)$ can be interpreted as the proportion of power of $x(t)$ explained by the linear relation with the power of $y(t)$ at a particular time and frequency band. It has the same meaning of a square correlation coefficient between two time series. Since the Morlet wavelet is complex, we may also obtain information about the possible delay in the relationship, that is information about which variable is leading the other one, by computing the phase difference. The

analysis of the phase or out of phase relationship allows us to get insights into the asymmetric association between the two series, which could be useful for making hypothesis about possible causal relationships. The phase difference is defined as follows:

$$\phi_{x,y}(f, \tau) = \tan^{-1} \frac{\Im(\langle W_{x,y}(f, \tau) \rangle)}{\Re(\langle W_{x,y}(f, \tau) \rangle)}, \quad (17)$$

where \Im indicates the imaginary part and \Re the real part. The phase difference varies cyclically between $-\pi$ and π over the duration of the component waveforms. Positive values suggest that is $x(t)$ leading $y(t)$ while negative values suggest the opposite situation. Values close to zero indicate that the relationship between the two series, if present, is symmetric.

2.2.5 Significance level

One can test whether the wavelet-based quantities, that is the spectra or coherence, observed at a particular time for a particular scale, are real features and not due to a random process with the same Markov transitions as the original time series. In our application, we perform hypothesis testing using the existing R functions written by [23] and available at the author's website. The functions are an advanced version of the **biwavelet** R package. Regarding the wavelet spectrum, one can compare the estimated sample spectrum with a background noise spectrum. To make such comparisons, statistical tests such as the point-wise [28], area-wise [30, 31], geometric [32], and cumulative area-wise [33] can be implemented. The point wise significant test proposed by [28] is the first and still mostly used method that allows placing wavelet analysis in a statistical hypothesis testing framework. In the point-wise approach, the statistical significance of wavelet quantities associated with points in a wavelet spectrum is assessed individually, without considering the correlation structure among wavelet coefficients. For wavelet power spectra of climate time series, theoretical red-noise spectra are the preferred noise background spectra against which sample wavelet power spectra are tested. Regarding coherence, more recent Monte Carlo methods are used to estimate the background noise spectra [34, 35]. We apply both the point-wise approach and the cumulative area-wise test developed by [23]. The second approach overcomes some drawbacks of the first one addressed in literature, like the frequent generation of many false positive results because of the simultaneous testing of multiple hypotheses [31, 32] and the occurrence of spurious results in clusters because of the correlations of the wavelet coefficients.

3 Analysis

3.1 Discrete wavelet and multiresolution analysis

Multiresolution analysis (MRA) permits a very detailed analysis by separating the signal into components at different scales. We apply the MODWT with

dyadic scale allowing us to decompose variations in the monthly series at scales of 1, 2, 4 months and so on. As introduced in Section 2.2.2, for a fixed level of decomposition J , the original time series \mathbf{X} can be reconstructed based on the wavelet coefficients as $\mathbf{X} = \sum_{j=1}^J \mathbf{D}_j + \mathbf{S}_J$. The analysis of monthly data with $J = 4$ gives a sequence of results which relate to variations at scales of 1, 2, 4 and 8 months. Extracting signal components at different resolutions amounts to decomposing variations in the data on different time scales, or equivalently in different frequency bands (different rates of oscillation). Accordingly, one can visualize signal variability at different scales, or frequency bands simultaneously. Detail components \mathbf{D}_j become progressively smoother since, in terms of frequency, the frequencies contained in the components become progressively lower. Figures 1 and 2 report, for each time series, the distribution of the estimated wavelet variances, calculated as the variance of the wavelet coefficients at that scale. It is interesting because it provides a decomposition of the time series variance $\sigma_{\mathbf{X}}^2$ on a scale by scale basis. The analysis reveals

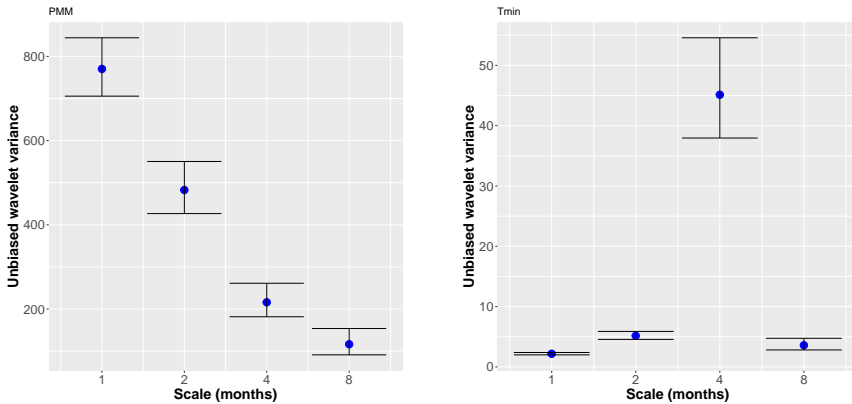


Fig. 1 Wavelet variance decomposition of monthly cumulated PMM (left) and monthly Tmin (right)

that temperature and precipitation have a different periodicity. While for the minimum, the maximum and the temperature range the main periodic component (that is, the scale contributing the most to the variance of the series) is clearly 4 months and the periodicity is thus close to the seasonality, for rain intensity the main periodic component is one month. Figures 3–6 show the wavelet detail series \mathbf{D}_3 for PMM, Tmin, Tmax and Trange, corresponding to the scale of 4 months previously detected as the main periodic component for temperature. As outline before, we can think \mathbf{D}_3 as the seasonal component in the data. We also report the wavelet detail series \mathbf{D}_1 (Figure 7) for PMM, as it is the main responsible for the variability in the PMM time series. The analysis reveals that the main oscillating component is nearly constant through time, both in amplitude and time location, for Tmin, Tmax and Trange. On the contrary, the seasonal behavior of the rain intensity is quite irregular with

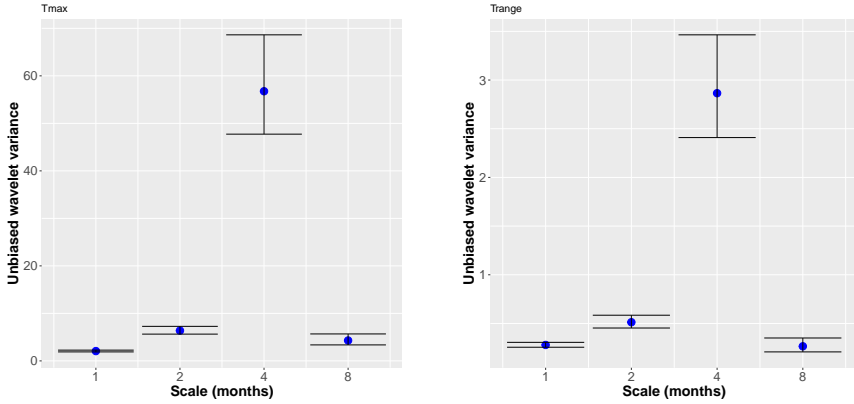


Fig. 2 Wavelet variance decomposition of monthly Tmax (left) and monthly average Trange (right)

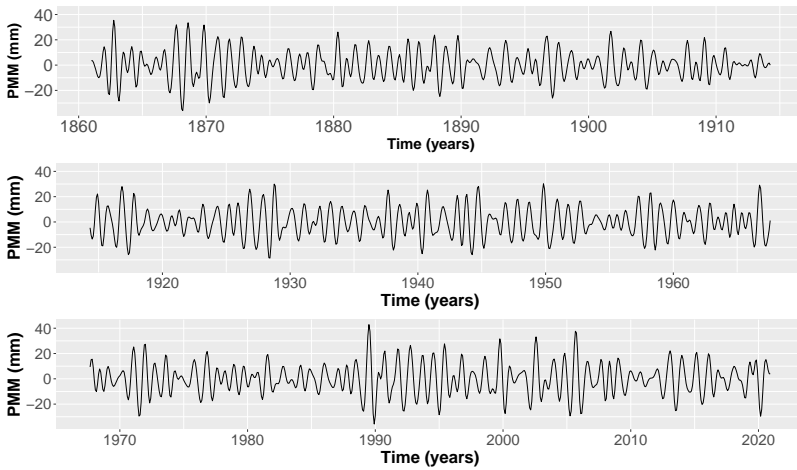


Fig. 3 Time series plot of D_4 for monthly cumulated PMM - scale 4 months

more frequent peaks in the last four decades. It is hard to identify changing behaviour or any specific time evolution in the considered period (Figure 3). However, if we analyse the monthly pattern D_1 (Figure 7) we note that extreme peaks are present in some years all over the observed period but the last two decades are characterized by the absence of nearly-zero amplitudes, quite frequent in the past years, and relative higher amplitudes of the oscillating component. We may conclude that, even though the seasonal behaviour of the rain intensity doesn't show an evident change in the last decades, the monthly behaviour has indeed changed in the mode of variability. The long term trend, that is the S_4 wavelet smooth for all series, is shown in Figure 8. We note an evident change in the trend component in all temperature series from around 1960 and a decrease in Trange over time. While both the minimum and the maximum temperature start increasing as ever before, the range

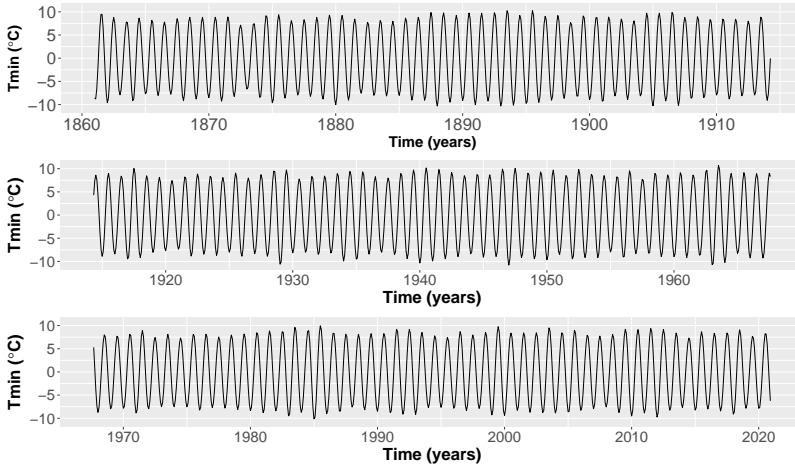


Fig. 4 Time series plot of D_4 for monthly Tmin - scale 4 months

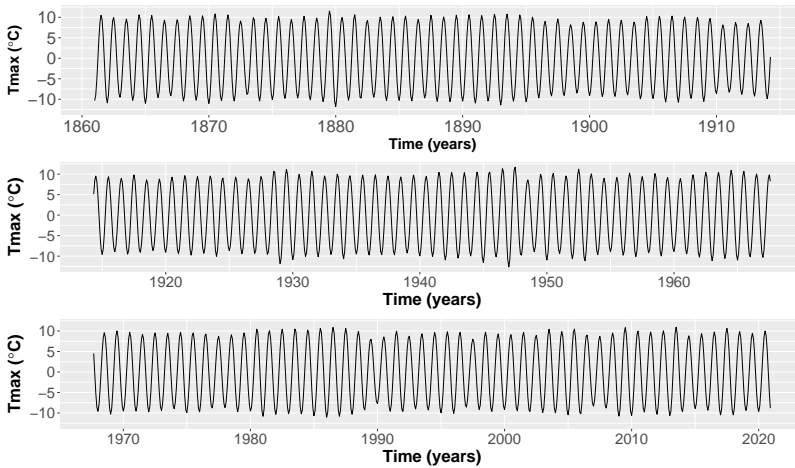


Fig. 5 Time series plot of D_4 for monthly Tmax - scale 4 months

temperature starts decreasing. Recent changes in the dynamics of the range temperature can be related to climate changes due to anthropogenic forcing [36–38]. The reduction of the range is associated to larger increases in minimum temperature than maximum temperatures over the same period and this difference has been attributed in literature to a number of factors such as urban heat, land use change, aerosols and greenhouse gases changes in solar irradiance [13, 39]. Different regions may be affected by different factors. In this study, we do not consider the possible anthropogenic causes but we find that, for the region of interest, temperatures changes are indeed present in the last 50 years, as supported by other local and global studies [39]. The large

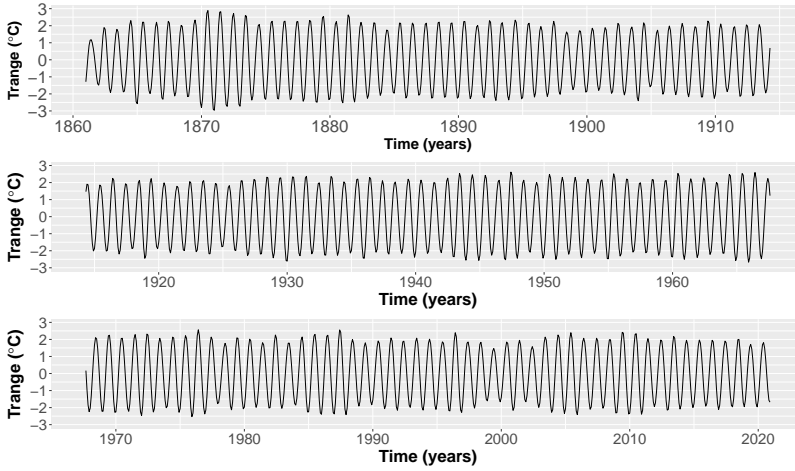


Fig. 6 Time series plot of D_4 for monthly Trange - scale 4 months

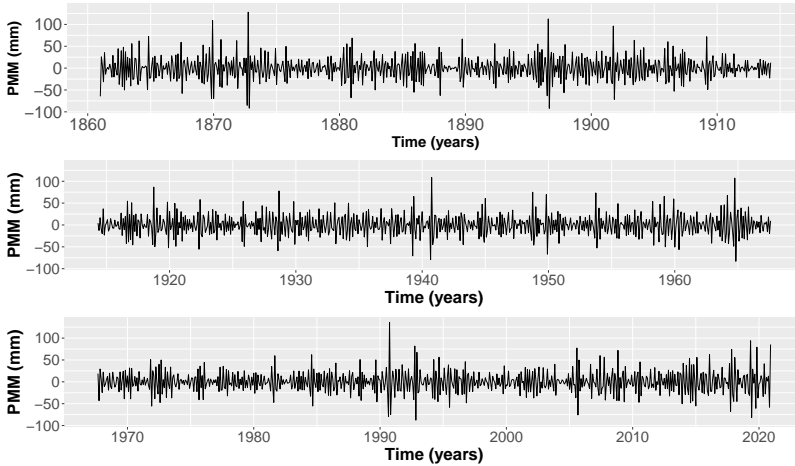


Fig. 7 Time series plot of D_1 for monthly cumulated PMM - scale 1 month

negative trend of the range temperature is an important meteorological indicator reflecting the instability of the weather very unlikely to have occurred due to internal variability or external climate forcing but rather associated to global dynamics related to human-induced changes.

3.2 Time dependent wavelet variance

The wavelet analysis reported in the previous section assumes variability to be constant over time. We can explore the time-dependent wavelet variance by choosing a smoothing window and by estimating the wavelet variance as a moving average of squared wavelet coefficients (note that the mean for the coefficients is zero). We chose a window of 12 months since the year is the

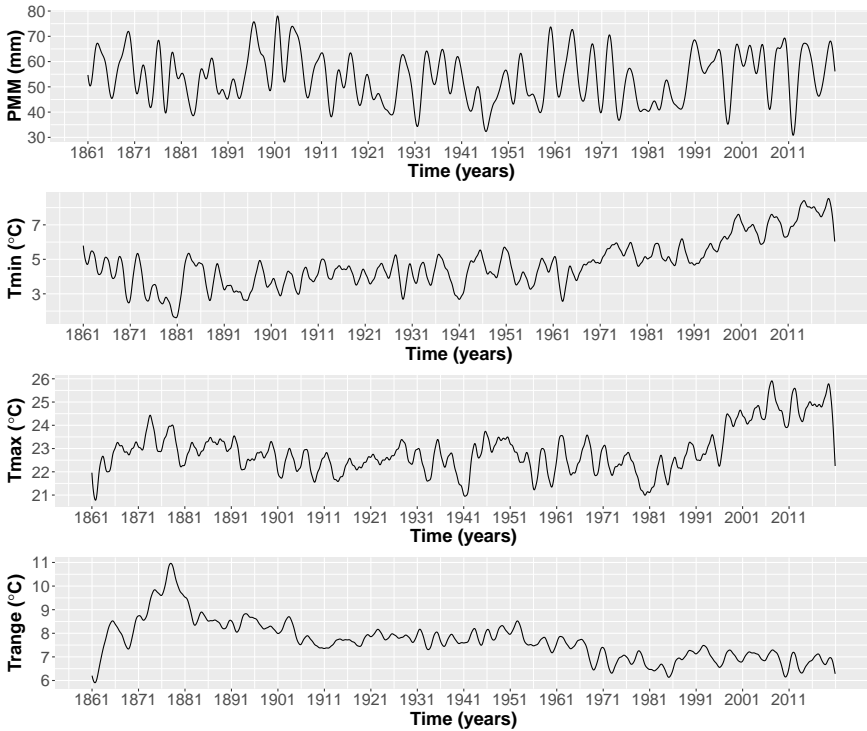


Fig. 8 Time series plot of S_4 for all series - scales 16 months and higher

natural period of geophysical processes occurring across seasons, like temperature and rain. The resulting time-dependent wavelet variances are reported in Figures 9–13. While Figures 3–6 allow us to investigate the changes in the mode of variability, from Figures 9–13 we may get insights into the changes of the magnitude of the variability across the last 160 years. We see that for rain intensity the variability has increased in the last 30 years, both considering the one month scale (responsible of the highest variability, Figure 9) and the seasonal scale (Figure 10). On the contrary, the temperature series show a decrease in variability in the last 30 years. For temperature, the highest variability is found during the period 1930–1960. This confirms that the minimum, the maximum and the temperature range in the last 50 years fluctuate less across seasons while the monthly and the seasonal cumulative precipitation depth is much more variable than before.

3.3 Continuous wavelet transform

Figures 14–17 show the wavelet power spectra obtained with continuous wavelet analysis (Eq. (13)). The vertical axis reports the wavelet scale (in years) while the horizontal axis is time (in years). The colour code for power ranges from dark blue (low values) to dark red (high values). The superimposed white area indicates the cone of influence that delimits the region influenced

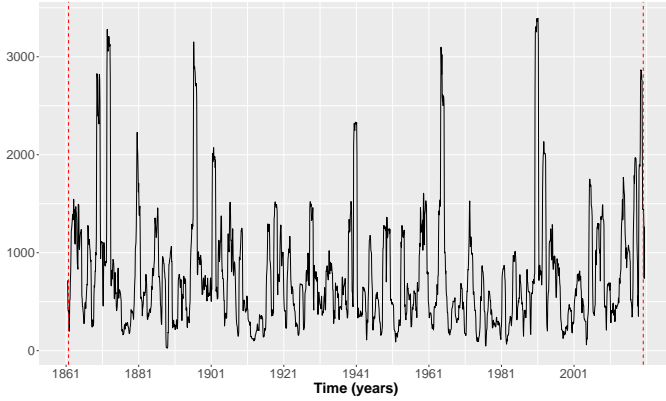


Fig. 9 Time dependent wavelet variance of PMM - scale 1 month. The dashed vertical lines represent areas affected by boundary effects

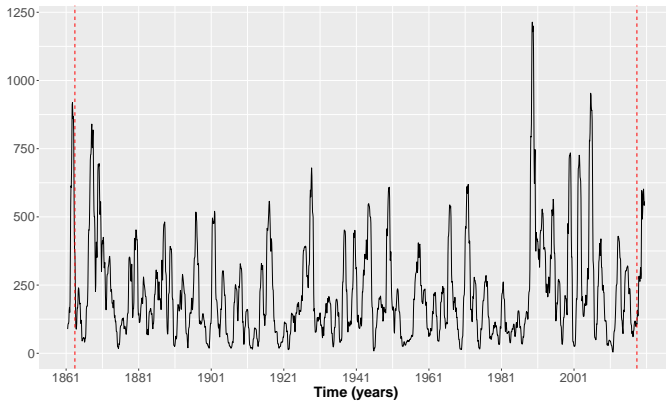


Fig. 10 Time dependent wavelet variance of PMM - scale 4 months. The dashed vertical lines represent areas affected by boundary effects

by edge effects. The thick black contours indicate areas (i.e. patches) significant at the $\alpha = 5\%$ level (following the cumulative area-wise testing by [23]). P-values associated with values within the contours are less than 5%. The analysis reveals a single persistent mode of variability of one year within the whole considered period, for temperature. It seems that temperature is not affected by transient features in annual or multi-annual scales. On the contrary, for rain there clearly exists a 32-year mode of variability that ends around 1980 (without considering the cone of influence) suggesting a potential change in the process generating rain at that time. Significant patches at scales of 2 and 4 years before 1900 and after 1950 respectively seem to be associated with singularity-like time domain features rather than periodicities, since they are intermittent.

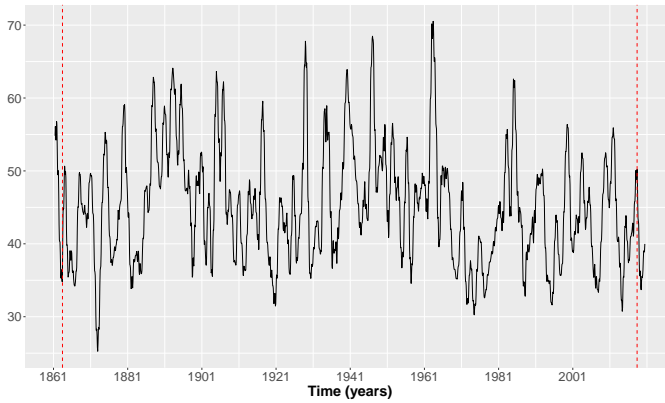


Fig. 11 Time dependent wavelet variance of Tmin - scale 4 months. The dashed vertical lines represent areas affected by boundary effects

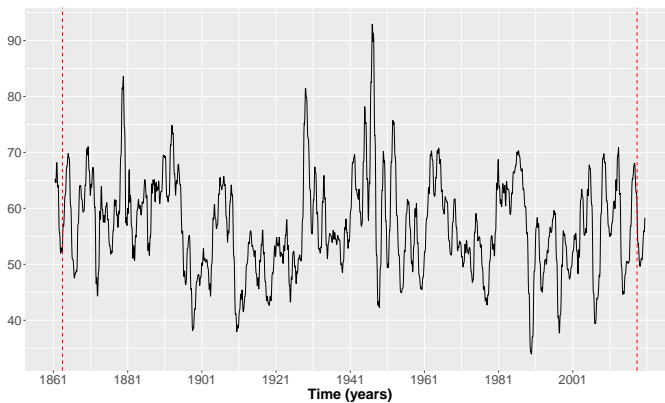


Fig. 12 Time dependent wavelet variance of Tmax - scale 4 months. The dashed vertical lines represent areas affected by boundary effects

3.4 Wavelet coherence

The analysis of the coherence (Eq. (16)) for two time series reveals areas with high common power. The value of the wavelet coherence can be thought of as a localized correlation coefficient in a time-frequency domain: its value in the $[0, 1]$ range provides information about how strong the association between the two series is, at each time point and time scale. The phase difference provides a measure of the lag difference between the two series at each time and scale. We can think about it as a suggestion of causality: if the phase difference is positive, it is the first series leading the second, and the other way around if the phase difference is negative. In the outcome, as for the power spectrum, the superimposed white area indicates the cone of influence, while thick black contours enclose areas (i.e. patches) significant at the $\alpha = 5\%$ level following the cumulative area-wise test.

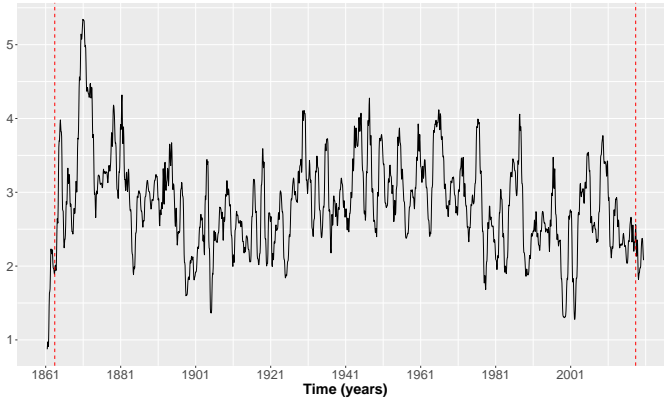


Fig. 13 Time dependent wavelet variance of Trange - scale 4 months. The dashed vertical lines represent areas affected by boundary effects

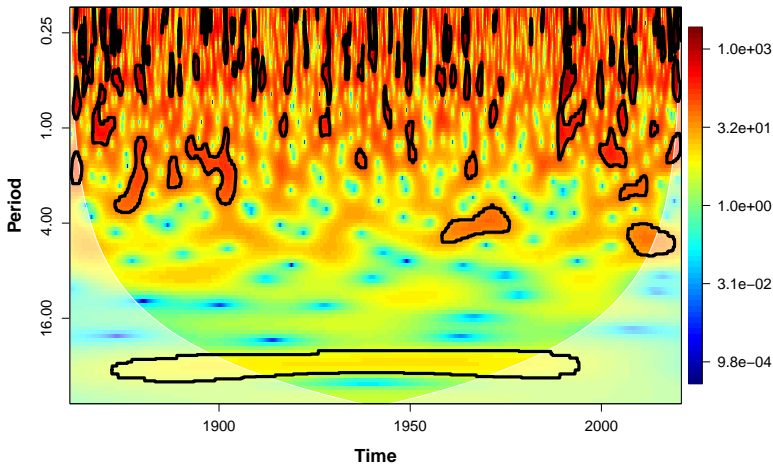


Fig. 14 Wavelet power spectrum of cumulated PMM

The top panels in Figures 18–20 show that an intermittent strong (significant) annual association between temperature and rain is present from 1861 until the year 2020. A significant inter-annual association is also found at higher scales but again it is not constant over time. For Tmax, it is particularly strong in the last 20 years on a scale of 2–8 years, and on a scale of 16 years over the period 1930–2000. The latter relationship is also found for Tmin. On the other hand, Trange shows a stronger (yet intermittent) relationship with rain than Tmin or Tmax on scales of 0.5 years and 2–6 years.

The bottom panels in Figures 18–20 show the phase difference. For easy of interpretation, we have added arrows wherever the coherence is above 0.8.

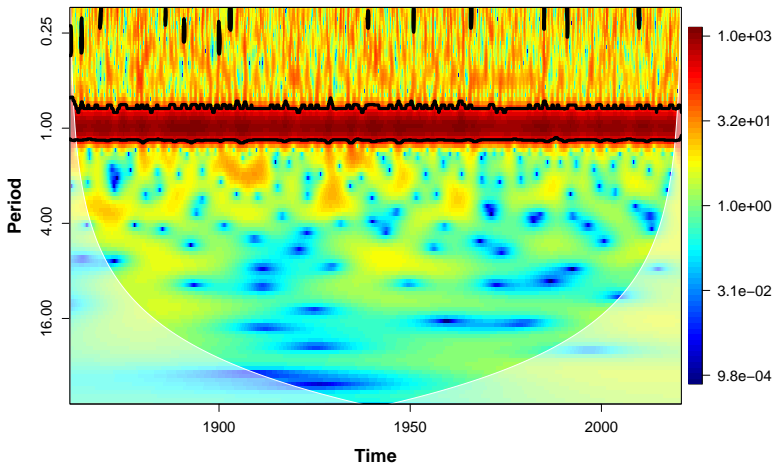


Fig. 15 Wavelet power spectrum of Tmin

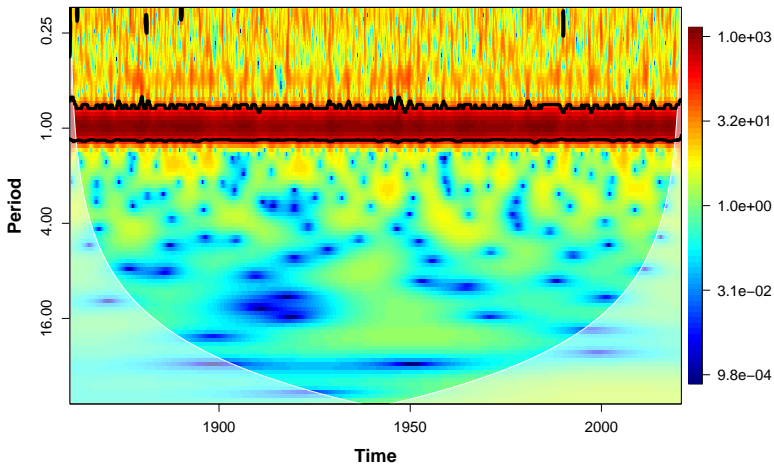


Fig. 16 Wavelet power spectrum of Tmax

It can be seen that the prevalent type of relationship, regardless of the scale, time period and couple of variables, is asymmetric, with temperature leading precipitation and not the other way around. This result can be generalized to a global scale, suggesting that global warming influences the other climatic variables.

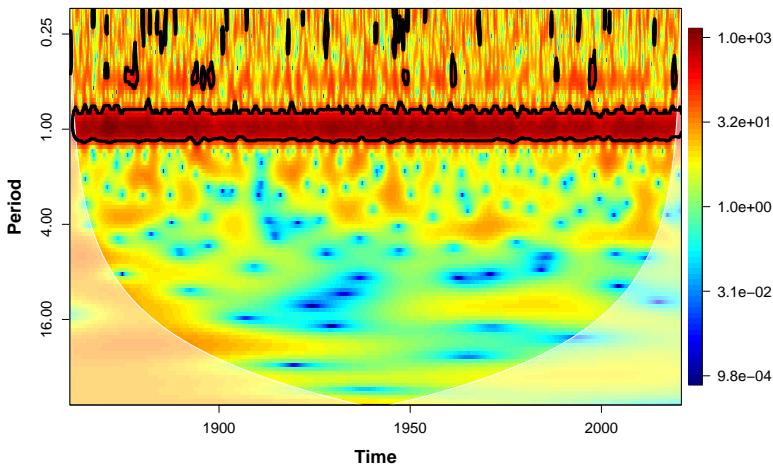


Fig. 17 Wavelet power spectrum of Trange

4 Discussion and Conclusions

Although it is commonly recognised that the mean air temperature is related to the increase in global carbon dioxide concentration, the dynamics of local trends due to local weather variables such as precipitation depth or due to local development remain unclear. Explaining the characteristic of local climate variables and the relationships among them is an important challenge emphasized by the increasing evidence that several ecological processes are affected by local climatic fluctuations. In this study, monthly series of air temperature and precipitation depth are examined over the period of time from 1861 to 2020 and a systematic analysis taking into account the essential features of non stationarity and time scale dependence is presented. Data are particularly relevant since long time series of observed and not reconstructed climatic variables are scarce in literature. Advanced statistical tools combining time and frequency domain such as wavelet analysis are used to determine and compare the internal variability of the series for different scales of time and to study the long-term patterns and the relationships between temperature and precipitation. Analysis of results suggests that the main periodic component leading the variability is one month for precipitation and 4 months for temperature, with a different cycling dynamic over the period 1861 to 2020 in rain and temperature range, and similar cycling dynamic in minimum and maximum temperature. Important discontinuities in the long-term trend start from 1981 for both rain and temperature. This marked change in the dynamic of the evolution of both climatic variables can be associated with endogenous or exogenous mechanisms such as local or global development (global CO₂, anthropogenic heating of urban areas). While rain shows the highest

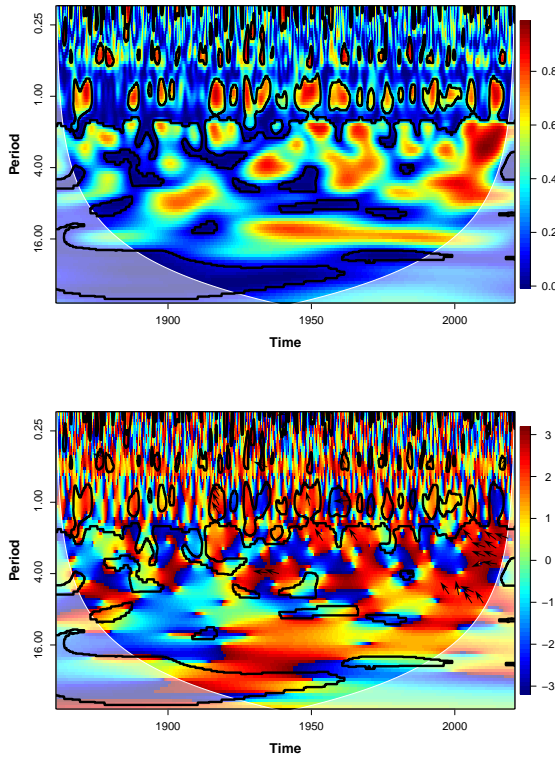


Fig. 18 Wavelet coherence (top) and phase (bottom) between Tmax and PMM

variability in the last two decades, temperature exhibits peaks of variability within the time interval 1930-1960. Within the same period, the relationship between temperature and precipitation is statistically significant considering multi-annual periods of about 16 years. From 2000, the association is highly significant considering multi-annual periods of 2-4 years. There is a strong significant relationship between temperature and precipitation on a yearly cycle but it is not constant over the time period under study. An important finding of this study is the different pattern of the minimum and maximum temperatures and the monthly average of daily range temperature in the last 50 years, consistent with recent works showing how climate change mostly influences temperature range [40, 41].

In conclusion, the present study highlights the following key points. Changes in temperature maximum and minimum values display different behavior than changes in temperature range. Temperature and precipitation display different timescales of the periodic components and persistent main mode and variances changing in time. Wavelet coherence analysis shows that the relationship between temperature and precipitation evolves in time and suggests that it is temperature driving rainfall and not the other way around.

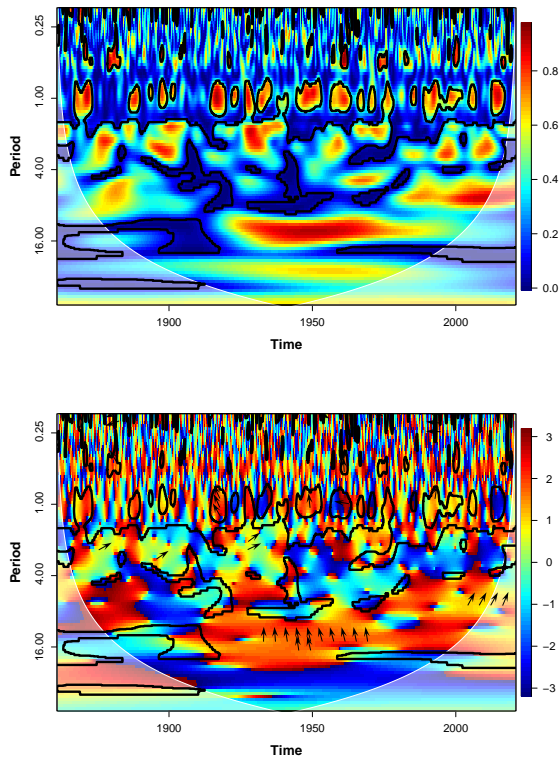


Fig. 19 Wavelet coherence (top) and phase (bottom) between Tmin and PMM

Declarations

The authors have no relevant financial or non-financial interests to disclose. The authors have no competing interests to declare that are relevant to the content of this article.

DATA AVAILABILITY

3. The datasets generated during and/or analysed during the current study are available from the corresponding author on reasonable request.

References

- [1] Easterling, D.R., Peterson, T.C., Karl, T.R.: On the development and use of homogenized climate data sets. *J. Clim.* **9**, 1429–1434 (1996)
- [2] Hansen, J.E., Lebedeff, S.: Global trends of measured surface air temperature. *J. Geophys. Res.* **92**, 13345–13372 (1987)
- [3] Hansen, J., Ruedy, R., Sato, M., Lo, K.: Global surface temperature

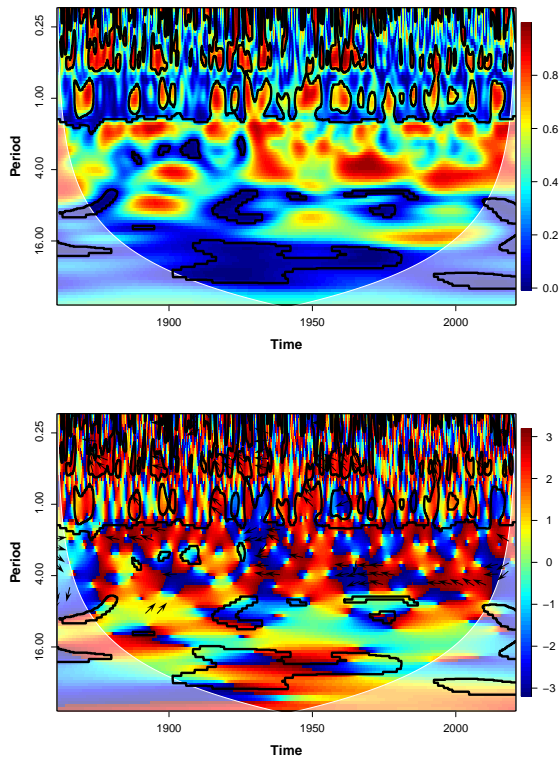


Fig. 20 Wavelet coherence (top) and phase (bottom) between Trange and PMM

range. *Reviews of Geophysics* **48**(4) (2010). <https://doi.org/10.1029/2010RG000345>

- [4] Thompson, D.W.J., Wallace, J.M., Jones, P.D., Kennedy, J.J.: Identifying signatures of natural climate variability in time series of globalmean surface temperature: Methodology and insights. *J. Clim.* **22**, 6120–6141 (2009)
- [5] Hansen, J., Johnson, D., Lacis, A., Lebedeff, S., Lee, P., Rind, D., Russel, G.: Climate impact of increasing atmospheric carbon dioxide. *Science* **213**(4511), 957–966 (1981)
- [6] Simmons, A.J., Willett, K.M., Jones, P.D., Thorne, P.W., Dee, D.P.: Low-frequency variations in surface atmospheric humidity, temperature, and precipitation: Inferences from reanalyses and monthly gridded observational data sets. *Journal of Geophysical Research: Atmospheres* **115**(D1) (2010). <https://doi.org/10.1029/2009JD012442>

- [7] Sutton, R., Suckling, E., Hawkins, E.: What does global mean temperature tell us about local climate? *Philosophical transactions. Series A, Mathematical, physical, and engineering sciences* **373** (2015). <https://doi.org/10.1098/rsta.2014.0426>
- [8] Woody, J., Lu, Q., Livsey, J.: Statistical methods for forecasting daily snow depths and assessing trends in inter-annual snow depth dynamics. *Environ. Ecol. Stat.* **27**, 609–628 (2020). <https://doi.org/10.1007/s10651-020-00461-5>
- [9] Torrence, C., Compo, G.P.: A parctical guide to wavelet analysis. *Bull. Am. Meteorol. Soc.* **79**, 61–78 (1998)
- [10] Percival, D.B., Walden, A.T.: *Wavelet Methods for Time Series Analysis*. Cambridge University Press, Cambridge (2000)
- [11] Gallegati, M.: A systematic wavelet-based exploratory analysis of climatic variables. *Climatic Change* **148**, 325–338 (2018)
- [12] Braganza, K., Karoly, D.J., Hirst, A.C., Mann, M.E., Stott, P.A., Stouffer, R.J., Tett, S.F.B.: Simple indices of global climate variability and change: Part i, variability and correlation structure. *Clim. Dyn.* **20**, 491–502 (2003)
- [13] Braganza, K., Karoly, D.J., Arblaster, J.M.: Diurnal temperature range as an index of global climate change during the twentieth century. *Geophys. Res. Lett.* **31** (2004). <https://doi.org/10.1029/2004GL01999>
- [14] Daubechies, I.: Orthonormal bases of compactly supported wavelet. *Communications on Pure and Applied Mathematics* **41(7)**, 909–946 (1988)
- [15] Akansu, A.N., Haddad, R.A., Caglar, H.: *Multiresolution Signal Decomposition: Transforms, Subbands, and Wavelets*. MA Academic Press, Boston (1992)
- [16] Akansu, A.N., Smith, M.J.: *Subband and Wavelet Transforms: Design and Applications* vol. 340. Springer, NY (1995)
- [17] Mallat, S.: *A Wavelet Tour of Signal Processing*. Ca Academic, San Diego (1999)
- [18] Elayouty, A., Scott, M., Miller, C., Waldron, S., Franco-Villoria, M.: Challenges in modeling detailed and complex environmental data sets: a case study modeling the excess partial pressure of fluvial CO₂. *Environmental and Ecological Statistics* **23(1)**, 65–87 (2016)

- [19] Mi, X., Rend, Z. H. Ouyang, Wei, W., Ma, K.: The use of the mexican hat and the morlet wavelets for detection of ecological patterns. *Plant. Ecol.* **179**, 1–19 (2005)
- [20] R Core Team: R: A Language and Environment for Statistical Computing. R Foundation for Statistical Computing, Vienna, Austria (2021). R Foundation for Statistical Computing. <https://www.R-project.org/>
- [21] Aldrich, E.: Wavelets: Functions for Computing Wavelet Filters, Wavelet Transforms and Multiresolution Analyses. (2020). R package version 0.3-0.2. <https://CRAN.R-project.org/package=wavelets>
- [22] Gouhier, T.C., Grinsted, A., Simko, V.: R Package biwavelet: Conduct Univariate and Bivariate Wavelet Analyses. (2021). (Version 0.20.21). <https://github.com/tgouhier/biwavelet>
- [23] Schulte, J.A.: Statistical hypothesis testing in wavelet analysis: theoretical developments and applications to indian rainfall. *Nonlin. Processes Geophys.* **26**, 91–108 (2019)
- [24] Lau, K.M., Weng, H.: Climatic signal detection using wavelet transform: how to make a time serie sing. *Bull. Am. Meteorol. Soc.* **76**, 2391–2402 (1995)
- [25] Daubechies, I.: Ten Lectures on Wavelets. SIAM monographs, Philadelphia (1992)
- [26] Cazelles, B., Chavez, M., Berteaux, D., Menard, F., Vik, J.O., Jenouvrier, S., Stenseth, N.C.: Wavelet analysis of ecological time series. *Oecologia* **156**, 287–304 (2008)
- [27] Donoho, D.L., David, L., Johonstone, J.M.: Ideal spatial adaptation by wavelet shrinkage. *Communications on Pure and Applied Mathematics* **81(3)**, 425–455 (1994)
- [28] Torrence, C., Webster, P.: Interdecadal changes in the esno-monsoon system. *J. Clim.* **12**, 2679–2690 (1999)
- [29] Chatfield, J.R.: The Analysis of Time Series: an Introduction. Chapman and Hall, London (1989)
- [30] Maraun, D., Kurths, J.: Cross wavelet analysis: significance testing and pitfalls. *Nonlin. Processes. Geophys.* **11**, 505–514 (2004). <https://doi.org/10.5194/npg-11-505-2004>
- [31] Maraun, D., Kurths, J., Holschneider, M.: Non-stationary gaussian processes in wavelet domain: definitions, estimation and significance testing.

- Phys. Rev. E. **75** (2007). <https://doi.org/10.1103/PhysRevE.75.016707>
- [32] Schulte, J.A., Duffy, C., Najjar, R.G.: Geometric and topological approaches to significance testing in wavelet analysis. *Nonlin. Processes Geophys.* **22**, 139–156 (2015). <https://doi.org/10.5194/npg-22-139-2015>
 - [33] Schulte, J.A.: Cumulative areawise testing in wavelet analysis and its application to geophysical time series. *Nonlin. Processes Geophys.* **23**, 45–57 (2016). <https://doi.org/10.5194/npg-23-45-2016>
 - [34] Schulte, J.A.: Wavelet analysis for non-stationary, nonlinear time series. *Nonlin. Processes Geophys.* **23**, 257–267 (2016). <https://doi.org/10.5194/npg-23-257-2016>
 - [35] Grinsted, A., Moore, J.C., Jevrejeva, S.: Application of the cross wavelet transform and wavelet coherence to geophysical time series,. *Nonlin. Processes Geophys.* **11**, 561–566 (2004). <https://doi.org/10.5194/hess-20-3183-2016>
 - [36] Stone, D.A., Weaver, A.J.: Daily maximum and minimum temperature trends in a climate model. *Geophys. Res. Lett.* **29(9)**(1356) (2002). <https://doi.org/10.1029/2001GL014556>
 - [37] Stone, D.A., Weaver, A.J.: Factors contributing to diurnal temperature range trends in twentieth and twenty-first century simulations of the cccma coupled model. *Clim. Dyn.* **12**, 2451–2473 (2003)
 - [38] Dai, A., Trenberth, K.E., Karl, T.R.: Effects of clouds, soil moisture, precipitation and water vapor on diurnal temperature range. *J. Clim.* **12**, 2451–2473 (1999)
 - [39] Makowski, K., Wild, M., Ohmura, A.: Diurnal temperature range over europe between 1950 and 2005. *Atmospheric Chemistry and Physics* **8**, 6483–6498 (2008)
 - [40] Kalnay, E., Cai, M.: Impact of urbanization and land-use change on climate. *Nature* **423**(6939), 528–531 (2003)
 - [41] Hua, L., Ma, Z., Guo, W.: The impact of urbanization on air temperature across china. *Theoretical and Applied Climatology* **93**(3), 179–194 (2008)